A terminal functionalization strategy reveals unusual binding abilities of anti-thrombin anticoagulant aptamers

Romualdo Troisi,[1] Claudia Riccardi,[1] Kévan Pérez de Carvasal,[2] Michael Smietana,[2] François Morvan,[2] Pompea Del Vecchio,[1] Daniela Montesarchio,[1] and Filomena Sica[1]

[1]Department of Chemical Sciences, University of Naples Federico II, 80126 Naples, Italy; [2]Institut des Biomolécules Max Mousseron, Université de Montpellier, CNRS, ENSCM, 34293 Montpellier, France

Despite their unquestionable properties, oligonucleotide aptamers display some drawbacks that continue to hinder their applications. Several strategies have been undertaken to overcome these weaknesses, using thrombin binding aptamers as proof-of-concept. In particular, the functionalization of a thrombin exosite I binding aptamer (TBA) with aromatic moieties, e.g., naphthalene dimides (N) and dialkoxynaphthalenes (D), attached at the 5′ and 3′ ends, respectively, proved to be highly promising. To obtain a molecular view of the effects of these modifications on aptamers, we performed a crystallographic analysis of one of these engineered oligonucleotides (TBA-NNp/DDp) in complex with thrombin. Surprisingly, three of the four examined crystallographic structures are ternary complexes in which thrombin binds a TBA-NNp/DDp molecule at exosite II as well as at exosite I, highlighting the ability of this aptamer, differently from unmodified TBA, to also recognize a localized region of exosite II. This novel ability is strictly related to the solvophobic behavior of the terminal modifications. Studies were also performed in solution to examine the properties of TBA-NNp/DDp in a crystal-free environment. The present results throw new light on the importance of appendages inducing a *pseudo*-cyclic charge-transfer structure in nucleic acid-based ligands to improve the interactions with proteins, thus considerably widening their potentialities.

INTRODUCTION

Nucleic acid-based aptamers are synthetic molecules with great potential in both therapeutic and diagnostic applications thanks to their peculiar binding abilities, which are strictly related to their structural organization.[1–3] Several aptamers are currently in different stages of clinical trials, and the search for new aptamer-based drugs, drug carriers, and even diagnostic tools is rapidly expanding.[4,5] In this context, recent strategies aim to broaden the aptamer applications by introducing in the backbone hydrophobic groups that compensate the low hydrophobicity of nucleic acids, thus expanding the variety of interactions between aptamers and target molecules.[6]

In the last years, particular attention has been paid to aptamers able to regulate the activity of human α-thrombin (thrombin), a serine protease with a key role in blood coagulation.[7,8] Similar to the other blood coagulation proteinases, thrombin specificity for substrate, inhibitor, and effector is mediated by the binding to exosites on the protein surface, which are physically separated from the catalytic site.[7] As concerns the inhibition of the thrombin activity, the anticoagulant aptamers interacting with the substrate recognition site, termed exosite I, are promising to such an extent that two of them have been considered for clinical trials[8]: TBA (also known as HD1) and NU172, that adopt a G-quadruplex and a mixed duplex/quadruplex structure, respectively.[9,10] A second class of aptamers that are able to recognize the heparin-binding site (exosite II) of thrombin has been also selected.[11,12] HD22 and Toggle families, DNA and RNA aptamers adopting duplex/quadruplex and stem-loop structures, respectively, are at the forefront in the thrombin exosite II recognition.[13,14] Despite their excellent binding abilities, these aptamers do not show anticoagulant properties, making them suitable candidates for the design of effective biosensors. Recently, several studies on the simultaneous binding of two aptamers at both thrombin exosites were performed, pointing out an aptamer-guided inter-exosite cooperativity.[15–18]

Thrombin binding aptamers are also often used as proof-of-concept in analyzing the effects of new chemical modifications on the properties of oligonucleotides. Indeed, despite the countless favorable properties of oligonucleotide aptamers, some non-negligible drawbacks, such as their low resistance to nucleases, greatly limit their use *in vivo* and do not allow their definitive consecration as drugs.[19] In the attempt to solve these issues, different strategies have been explored, particularly aiming at optimizing both TBA and NU172 aptamers, by insertion of chemical modifications at the level of the sugar-phosphate backbone and/or of key residues of their sequences.[20–32] Recently, some of us developed innovative functionalization methods
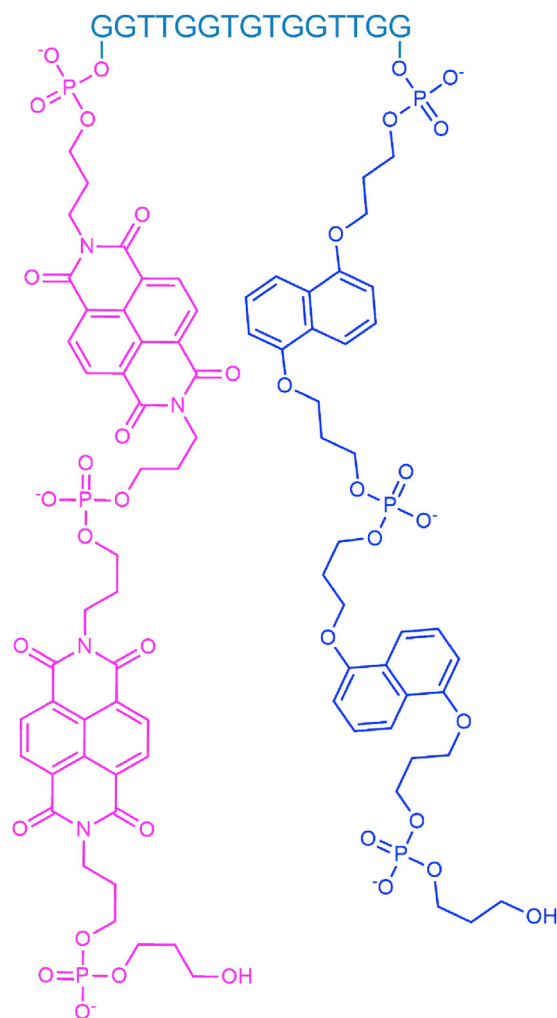
Figure 1. Chemical structure of TBA-NNp/DDp

The oligonucleotide sequence is in deep teal, and the 5′ and 3′ terminal appendages are in magenta and blue, respectively.

based on the cyclization or *pseudo*-cyclization of anti-thrombin aptamers, that led to extraordinarily stabilized oligonucleotides, some of which showed preserved, or even improved inhibition properties.[33–36] This is the case of the *pseudo*-cyclic TBA analogue named TBA-NNp/DDp (Figure 1), in which the 3′ and 5′ ends of the 5′-GGTTGGTGTGGTTGG-3′ sequence have been respectively conjugated with two electron-rich 1,5-dialkoxy naphthalene (DAN, D) and two electron-deficient 1,8,4,5-naphthalenetetra-carboxylic diimide (NDI, N) moieties, provided with terminal 1,3-propanediol phosphodiester groups (p).[36] TBA-NNp/DDp exhibited a considerable improvement of the thermal stability and nuclease resistance, coupled with a moderate increase in anticoagulant activity with respect to unmodified TBA. Circular dichroism experiments performed in the presence of K^+ ions showed that the melting temperature (T_m) of the G-quadruplex domain of TBA-NNp/DDp is 11°C higher than TBA. Moreover, the half-life in fetal bovine serum and

the anticoagulant activity of this *pseudo*-cyclic aptamer proved to be respectively amplified by 4.5 and 1.2 times compared with those of the parent aptamer.

Encouraged by these promising results and eager to obtain an in-depth structural characterization of this intriguing *pseudo*-cyclic TBA analogue, we carried out a comprehensive crystallographic analysis of the complex between thrombin and TBA-NNp/DDp. In particular, we solved the structure of this complex in four different crystal forms, obtaining unprecedented structural data on a secondary interaction of the TBA-like aptamer with thrombin exosite II. Interestingly, the crystal packing analysis has revealed the ability of the aromatic appendages to make contacts with hydrophobic patches of the protein surface thanks to their solvophobic behavior. These data clearly suggest that the introduction of hydrophobic portions in an oligonucleotide sequence represents a powerful strategy to shape the contact surface with the target molecule. Spectroscopic, calorimetric, and electrophoretic studies were also performed to deeply investigate in solution the folding and binding properties of this TBA analogue.

RESULTS

Crystallographic analysis

The crystallographic analysis of the complex between thrombin and TBA-NNp/DDp involved four crystals (Figure S1) grown in different conditions, here named α, β, γ, and δ (Table 1 and Table S1), and belonging to $P6_4$, $P3_121$, $P2_1$, and $P3_221$ space groups, respectively. The crystals diffract X-ray up to 3.18, 2.00, 3.03, and 2.50 Å resolution, respectively. In all crystal forms, a TBA-NNp/DDp molecule interacts with the thrombin exosite I. In particular, in the crystal form α, a standard 1:1 thrombin-aptamer complex is found (Figure 2A). The asymmetric units of the crystals grown in conditions β and γ contain one (Figure 2B) and two ternary complexes (Figure 2C), respectively, in which thrombin is sandwiched between two TBA-NNp/DDp molecules, one for each exosite. In the case of crystal form δ (Figure 2D), the discontinuous residual electron density centered on the crystallographic 2-fold axis and close to exosite II (Figure S2) was reasonably interpreted by considering half occupancy for a TBA-NNp/DDp molecule, alternatively bound to exosite II of two symmetry-related complexes. Thus, the crystal contains equimolar amounts of 1:1 and 1:2 thrombin-aptamer complexes.

Aptamer structure

Regardless of the binding site and the crystal form, TBA-NNp/DDp adopts a well-defined elongated structure (Figure 3). The oligonucleotide domain folds in a TBA-like antiparallel G-quadruplex,[9] in which guanines 2, 5, 11, 14 and 1, 6, 10, 15 form G-tetrad I and II, respectively. A potassium ion is sandwiched between the two tetrads that are connected by a TGT (Thy7-Gua8-Thy9) and two TT (Thy3-Thy4 and Thy12-Thy13) loops. Thy4 and Thy13 of the TT loops are involved in intramolecular stacking interactions on G-tetrad I, while Thy3 and Thy12 interact with the protein (see next paragraphs). In all the present structures, the electron density in the TGT loop region is not well defined, suggesting a high mobility of this segment, whose

Table 1. Crystal data

	Crystal form α	Crystal form β	Crystal form γ	Crystal form δ
Crystallization condition	46% v/v Tacsimate™ pH 7.0	20% w/v PEG 4000 20% v/v 2-propanol 0.1 M trisodium citrate pH 5.6	25% w/v PEG 3350 0.2 M ammonium acetate 0.1 M Bis-Tris pH 6.5	30% w/v PEG 3350 0.2 M sodium malonate pH 7.0
Cryoprotection	20% v/v glycerol	–	25% v/v glycerol	25% v/v glycerol
Space group	P6$_4$	P3$_1$21	P2$_1$	P3$_2$21
Unit-cell parameters				
a, b, c (Å)	152.91, 152.91, 79.49	76.60, 76.60, 129.38	76.62, 114.86, 83.44	75.87, 75.87, 146.90
α, β, γ (deg)	90.00, 90.00, 120.00	90.00, 90.00, 120.00	90.00, 117.25, 90.00	90.00, 90.00, 120.00
V$_M$ (Å^3 Da^{-1})	6.20	2.20	3.28	2.62
No. of molecules in the asymmetric unit	One 1:1 thrombin-aptamer complex	One 1:2 thrombin-aptamer complex	Two 1:2 thrombin-aptamer complexes	Half 1:1/Half 1:2 thrombin-aptamer complex
Solvent content (%)	81.8	48.6	65.5	56.9

conformation is also affected by the presence of the terminal modifications (Figure S3). As concerns the latter ones, the two 1,8,4,5-naphthalenetetra-carboxylic diimide (NDI) and the two 1,5-dialkoxy naphthalene (DAN) moieties capitalize their charge-transfer interactions to alternately stack on top of each other, self-assembling in a hetero duplex domain delineated by NDI/DAN/NDI/DAN alternation (Figure 3). The first NDI at the 5' end in turn stacks on Gua1 and Gua15 of the G-tetrad II of the G-quadruplex domain. This continuous stacking between the oligonucleotide domain and terminal groups generates a compact architecture resembling that observed in the case of the exosite I-binding aptamers with a mixed duplex/quadruplex structure.[10,37] Only a few patches of electron density in correspondence of the terminal 1,3-propanediol phosphodiester groups are evident in almost all the crystal forms, thus indicating a high flexibility of these regions. In all cases, the aptamer terminal groups play a significant role in the crystal packing (Figure S4). In crystals α, β, and δ, they are involved in interactions with symmetry-related thrombin molecules. In crystal γ with two complexes in the asymmetric unit, the aptamers form end-stacking interactions in such a way as to preserve the charge-transfer driven alternation of NDI and DAN moieties (Figure 4). This construction requires that the terminal DAN group of the two interacting oligonucleotides is alternately disordered in the solvent.

Interaction of TBA-NNp/DDp with exosite I

Similar to TBA,[9] TBA-NNp/DDp binds the thrombin exosite I with the two TT loops by firmly gripping the protruding protein region from Arg73 to Ile79 (Figure S5). A thymine of a TT loop is located in the hydrophobic crevice of the protein surface formed by the phenyl ring of Tyr117 and the side chains of Ile24 and Ile79 and forms a hydrogen bond with the Glu77 side chain. Conversely, a thymine of the second TT loop interacts with Tyr76 via π-π stacking. The thymines not involved in these interactions, i.e., Thy4 and Thy13, form hydrogen bonds with the Arg75 side chain. Similar to unmodified TBA,[9,38] TBA-NNp/DDp is able to recognize thrombin exosite I in two alternative orientations related by a 180° rotation around the approximate G-quadruplex 2-fold axis (Figure S6). Indeed, in crystals

α and β, Thy3 stacks with Tyr76 and Thy12 occupies the hydrophobic crevice, while in the other crystals the positions of the two thymines are reversed. A detailed comparison of the interactions between TBA-NNp/DDp or TBA and exosite I in terms of buried area, interface residues, and hydrogen bonds is reported in Table S2.

Interaction of TBA-NNp/DDp with exosite II

Thrombin exosites I and II differ in their biological and structural features.[7] In particular, exosite I comprises a localized region of the protein surface, essentially formed by the Arg73-Ile79 loop, whereas exosite II is large and encompasses residues Tyr89-Arg101, Arg126-Leu130, Glu164-Lys169, and Phe232-Phe245. The unexpected interaction of TBA-NNp/DDp with exosite II, observed in crystals β, γ, and δ (Figure 2), involves a localized region of this exosite (residues Tyr89-Arg97 and Trp237-Phe245), which is embraced by the two TT loops (Figure S5). Noteworthy, TBA-NNp/DDp uses the same structural motif, the TT loops, for the binding to the two different protein regions. In detail, both Thy4 and Thy13 that stack on G-tetrad I interact with Arg93 side chain via hydrogen bonds. The other two thymine residues (Thy3 and Thy12) occupy two different crevices of the exosite II surface. A crevice is formed by the Asn95 and the side chains of Trp96 and Arg97, while the other is delimited on one side by Tyr89, Ile90, and Pro92 and on the other by the side chains of Trp237, Lys240, Val241, Gln244, and Phe245 (Figure 5). These thymines are held in these positions by hydrogen bonds involving either the protein backbone or side chains. A detailed summary of the buried area, the interfacing residues, and the hydrogen bonds involved in the binding of TBA-NNp/DDp with exosite II is reported in Table S3.

The comparison of the binding of TBA-NNp/DDp with that of aptamers that selectively recognize the thrombin exosite II shows that the TBA analogue is able to mate with a different section of the exosite with respect to that occupied by Toggle-25t, but with the same region as the G-quadruplex domain of HD22_27mer (see paragraph "Recognition of exosite II: TBA-NNp/DDp versus other aptamers" in the supplemental information, Figures S7–S9, and Table S4).
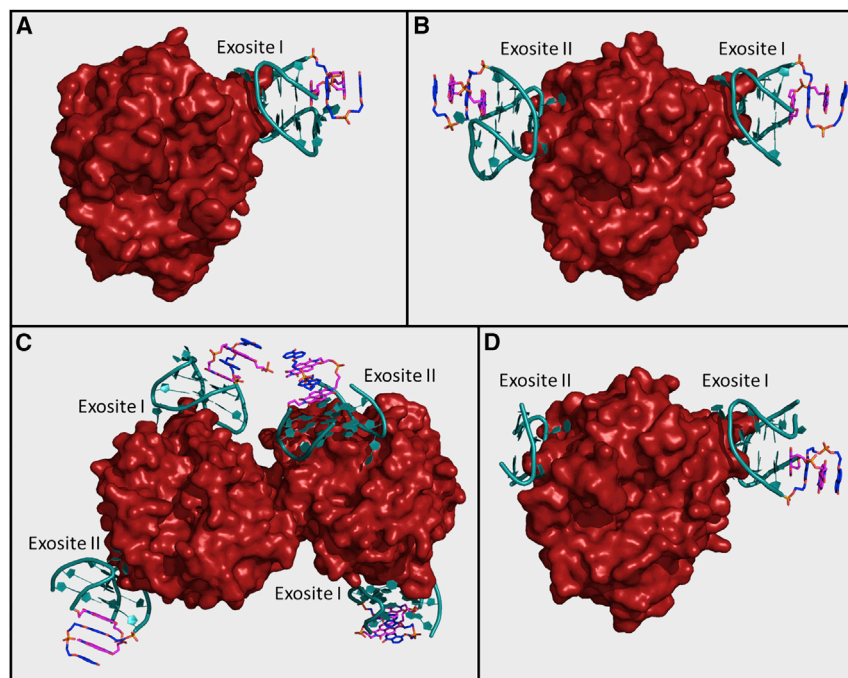
Figure 2. Thrombin-TBA-NNp/DDp complexes

Cartoon/surface representations of thrombin-TBA-NNp/DDp complexes in the asymmetric units of (A) crystal α, (B) crystal β, (C) crystal γ, and (D) crystal δ. Thrombin is red and oligonucleotide domain, NDIs, and DANs of TBA-NNp/DDp are in deep teal, magenta, and blue, respectively.

at 410 nm (Figure S12), in the proximity of NDI visible band, provided comparable T_m values of 67°C (Table 2), which are significantly higher ($\Delta T_m = 15$°C) than that reported for the unmodified aptamer.[39] This T_m value was further confirmed by DSC results (Table 2 and Figure S13), thus suggesting a global cooperative one-step unfolding process that correlates well with the compact structure of TBA-NNp/DDp found in the crystal state. The analysis of the thermodynamic parameters (Table 2) obtained by the DSC profile of the TBA analogue shows that the $\Delta H°$ and $\Delta S°$ values are quite comparable to those previously determined in the same conditions for the parent aptamer.[39] The only difference is the small increase of the enthalpic contribution for the modified TBA, which can be reasonably due to the additional interactions involving the 5' and 3' end appendages.

Electrophoretic analysis of the interaction of TBA-NNp/DDp with thrombin

The binding of TBA-NNp/DDp with thrombin at different aptamer-protein molar ratios (1:0.5, 1:1, and 1:2) was analyzed in comparison with unmodified TBA by EMSA analysis—a highly sensitive and widely used method to study protein–nucleic acid interactions[40]—under non-denaturing conditions (Figure 6).

The gels were subjected to a double-staining procedure, using first a staining specific for nucleic acids (Stains-All, Figure 6A) and then one specific for proteins (Coomassie, Figure 6B). Both unmodified TBA (lane 1) and TBA-NNp/DDp (lane 5) showed a single band on the gel, indicative of unimolecular species, with a migration ability in agreement with previous results.[36] Indeed, TBA-NNp/DDp exhibited a slightly increased electrophoretic mobility with respect to its parent aptamer, indicative of a more compact G-quadruplex structure.

EMSA analysis revealed a similar behavior for TBA and TBA-NNp/DDp, which in the presence of the protein (Figure 6A, lanes 2–4 for TBA and 6–8 for TBA-NNp/DDp), formed new retarded bands, attributable to the corresponding aptamer-protein complexes, as evidenced after nucleic acid staining. In detail, the 1:1 aptamer-thrombin mixtures (Figure 6A, lanes 2 and 6, respectively) showed a residual band of free, unbound aptamers, calculated as 25% and 47%, respectively for TBA and TBA-NNp/DDp (Figure S14). In the presence of a 2-fold excess of thrombin, the aptamer bands completely disappeared (Figure 6A, lanes 3 and 7, respectively for TBA and TBA-NNp/DDp).
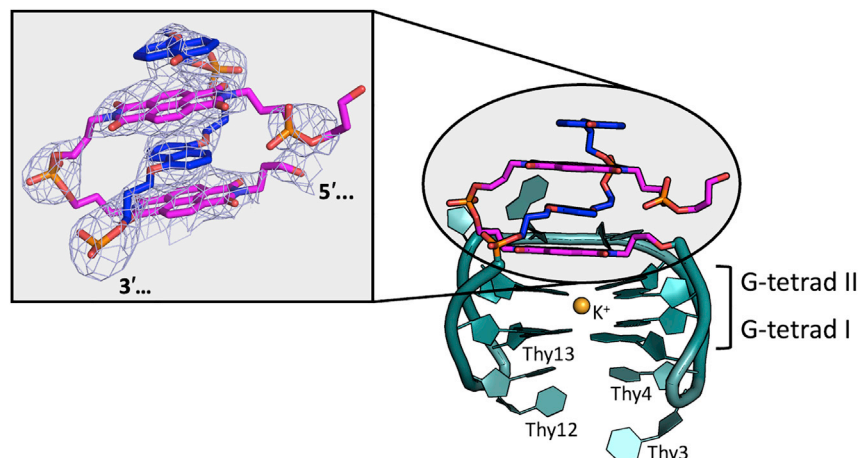
Finally, as observed in the case of the binding with exosite I, the *pseudo* 2-fold axis of the aptamer G-quadruplex region allows TBA-NNp/DDp to interact with exosite II in two alternative orientations (Figure S10). Indeed, in crystals β and δ, Thy12 is surrounded by Asn95, Trp96, and Arg97, and Thy3 is located near the C-terminal residues. The positions of the two thymine residues are reversed in crystal γ.

Interestingly, in the crystal form δ, the exosites II of two complexes face each other across a crystallographic 2-fold axis with an intervening aptamer that is alternately linked to either one of the two sites, so that the crystal contains a binary and a ternary complex.

Studies of TBA-NNp/DDp in solution

In order to investigate if the compact structural organization of the NDI and DAN moieties, linked at the 5' and 3' ends of the modified TBA, is preserved in solution, a thermal denaturation analysis of the free aptamer by CD, UV-Vis spectroscopies and differential scanning calorimetry (DSC) was performed in comparison with unmodified TBA. Furthermore, a comparison of the thrombin binding ability of TBA-NNp/DDp and the parent aptamer was performed by electrophoretic mobility shift assays (EMSA).

Analysis of the unfolding process of TBA-NNp/DDp

The thermal stability of TBA-NNp/DDp was evaluated by following the unfolding process of the two structural elements of the aptamer, the G-quadruplex domain and the stacked terminal appendages by CD and UV measurements, respectively. The analysis of the temperature-induced variation of the CD signal of the antiparallel G-quadruplex domain at 295 nm (Figure S11) and of the absorbance

with respect to each aptamer (Figure 6B, lanes 3 and 7, respectively for TBA and TBA-NNp/DDp), the bands of the unbound protein were clearly visible, having the same electrophoretic mobility as the band of the free protein used as control, and confirmed a similar behavior for TBA and TBA-NNp/DDp. This allowed also excluding the binding of the modified aptamer to more than one protein molecule, analogous to what was observed for the parent aptamer. On the other hand, when complexed with the aptamers, the thrombin band exhibited a detectable change in its mass-to-charge ratio and thus in its migration ability.

In all cases, TBA-NNp/DDp-thrombin complexes showed a lower electrophoretic migration than the TBA-thrombin ones. This finding is in line with the tendency of these complexes to form aggregates of high molecular weight, which is related to the solvophobicity of the oligonucleotide end-modifications.

Overall, EMSA studies suggested that, in solution, TBA-NNp/DDp preferentially interacts with thrombin with a TBA-like 1:1 stoichiometry.

In turn, the 1:0.5 aptamer-thrombin molar ratio mixtures (Figure 6A, lanes 4 and 8, respectively, for TBA and TBA-NNp/DDp) showed only a low amount of the aptamer-protein complexes along with a major amount of both free oligonucleotides in solution (determined as 58% and 67%, respectively, for TBA and TBA-NNp/DDp, Figure S14), suggesting that in both cases no more than one aptamer molecule is bound to thrombin.

Coomassie staining in the tested electrophoretic conditions showed a sharp band for free thrombin (lane 9). When used in molar excess

DISCUSSION

In the continuous effort to overcome the limits of oligonucleotide-based drugs and biosensors, a detailed structural characterization can facilitate the rational design of chemical modifications and reveal unexpected new properties. In this context, we have performed a detailed investigation of the structure of the recently proposed *pseudo*-cyclic TBA analogue named TBA-NNp/DDp. The diffraction data measured on four different crystal forms, grown from slightly different crystallization solutions, showed that TBA-NNp/DDp can either be engaged as a binary complex with thrombin in the crystal form α, or as a ternary complex in the crystal forms β and γ, or even as a binary and a ternary complex altogether in the mixed form δ. It should be recalled that previous studies performed on TBA, both in the solid-state and in solution,[9,31,41–44] have concordantly shown that TBA forms a 1:1 complex with thrombin. In this complex, the aptamer is specifically bound at the exosite I of the protein with the two TT loops firmly gripping the protruding protein region from Arg73 to Ile79. As expected, the oligonucleotide sequence that TBA-NNp/DDp shares with the parent aptamer, adopts the same antiparallel G-quadruplex structure including the TT loops binding motif. Indeed, the TBA analogue binds thrombin at the exosite I in all the four structures in a manner that is practically identical to that observed in the thrombin-TBA complex. This result clearly indicates
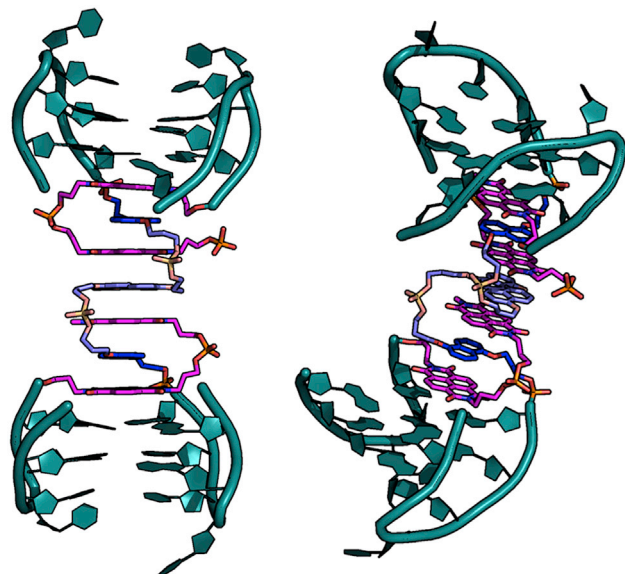

Figure 4. Views of the stacking interactions between two TBA-NNp/DDp molecules formed in the crystal γ

Oligonucleotide domain, NDIs, and DANs of TBA-NNp/DDp are in deep teal, magenta, and blue, respectively. The terminal DAN groups that alternately stack between the terminal NDI groups of two symmetry-related TBA-NNp/DDp molecules are in light colors.
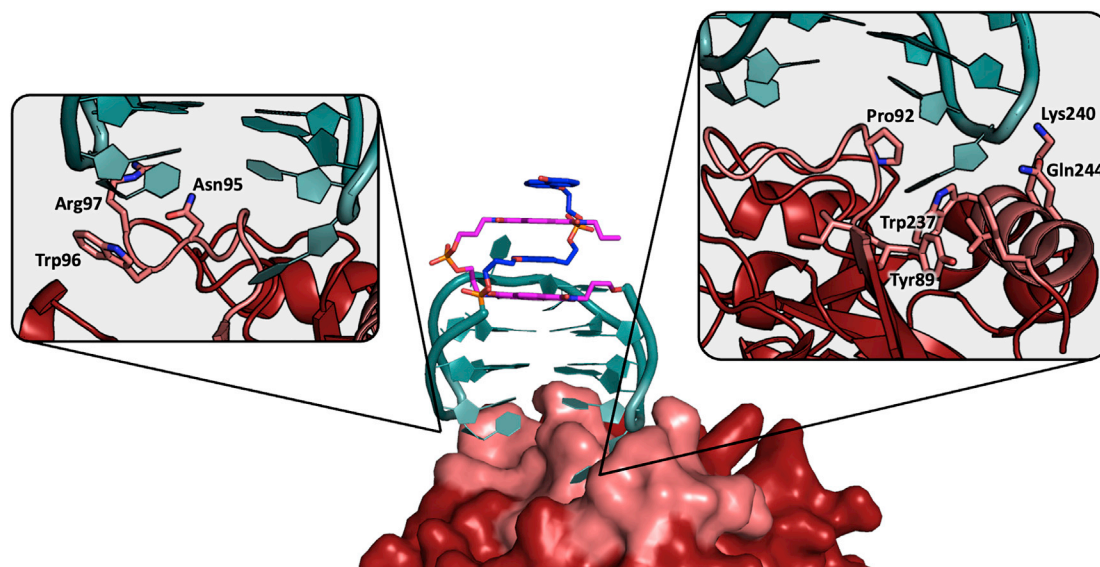
Figure 5. Aptamer-exosite II interactions
Cartoon representation of TBA-NNp/DDp interactions with a localized region of thrombin exosite II (light red). Oligonucleotide domain, NDIs, and DANs of TBA-NNp/DDp are in deep teal, magenta, and blue, respectively. On the sides, views of the residues forming the two crevices occupied by two thymines of the aptamer.

that the additional end groups do not impair the known binding interactions of TBA. In addition to its interaction with exosite I, some experimental results, such as aggregation data of aptamer-functionalized gold nanoparticles triggered by thrombin in solution,[45,46] indicated that TBA is involved in multiple interaction sites with thrombin. In particular, a secondary low-affinity interaction in the vicinity of exosite II has been suggested, although not fully described, and never observed in the crystalline state. Rather unexpectedly, in all the crystal forms of TBA-NNp/DDp complexed with thrombin, except for α, a ternary complex is found in which a second aptamer is bound at the exosite II. This is a more extended site with respect to exosite I, and is largely preferred by more complex ligands, as in the case of the mixed duplex/quadruplex aptamers that can efficiently cover the whole area of the site.[14] In particular, TBA-NNp/DDp interacts with a localized region of exosite II (the G4_A-region; see supplemental information) in a highly conservative manner with respect to the HD22_27mer quadruplex moiety. This finding qualifies this exosite II region as an efficient anchoring site for a TBA-like G-quadruplex construct, revealing a putative secondary

binding site also for TBA, although with a much lower affinity with respect to TBA-NNp/DDp.

In order to understand the reason for the different behavior of TBA and TBA-NNp/DDp, the role of the end groups in the TBA analogue should be briefly analyzed. As previously mentioned, the phosphodiester-linked NDI and DAN appendages at 5′ and 3′ ends, respectively, adopt a pleated fold exposed to the solvent on the other side of antiparallel G-quadruplex structure with respect to the TT loops. Besides that, the electronic complementarity, charge transfer, and solvophobic effects of NDI and DAN moieties drive the formation of the NDI/DAN/NDI/DAN stacking motif that ensures a very stable alternation of NDI and DAN moieties protruding out of the G-quadruplex molecular shape,[47–51] far away from the TT binding loops. Although this structural motif does not sensibly perturb the adhesion capacity of the TT loops, it does modify the overall hydration properties of the aptamer by increasing its hydrophobic character.[50,52] In this respect, the present crystal data are particularly rich of useful information regarding the properties of this TBA variant, which can throw light on its behavior in solution. In the solid phase α, which hosts only the binary complex, the solvent content is considerably high, i.e., almost double with respect to the other crystal forms (Table 1). The hydrophobic end groups of the aptamer are involved in several nonspecific contacts with the protein (Figure S15A), whereas the putative second binding site at exosite II is fully exposed to the solvent, facing a large cavity that could easily host a second aptamer (Figure S16). On the other hand, in the crystal forms containing the ternary complex, the crystal packing presents much smaller solvent cavities and is organized so to minimize the contacts of the hydrophobic end-chain groups with the solvent. This escaping tendency also produces in these crystal forms nonspecific packing interactions

Table 2. Melting temperature values of the unfolding process of TBA-NNp/DDp determined with different techniques

	CD	UV-Vis	DSC		
	T_m (°C)	T_m (°C)	T_m (°C)	ΔH_m° (kJ mol^{-1})	ΔS_m° (kJ mol^{-1} K^{-1})
TBA-NNp/DDp	67 ± 1	67 ± 1	66.1 ± 0.5	115 ± 6	0.34 ± 0.02
TBA[39]	52 ± 1	–	53.0 ± 0.5	99 ± 10	0.30 ± 0.03

The thermodynamic parameters obtained by the analysis of the DSC profile are also reported. Values for TBA are reported for comparison.
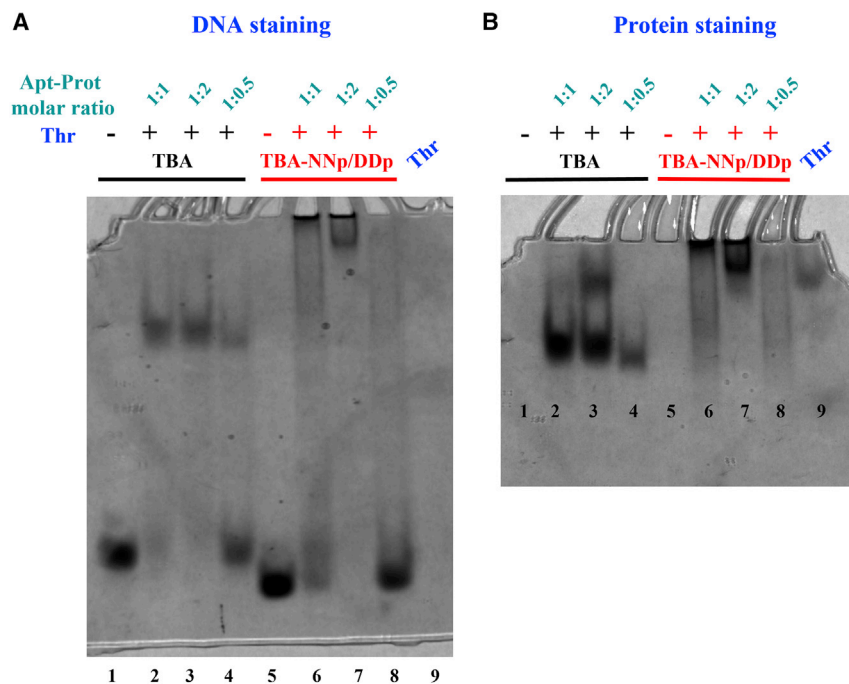
Figure 6. EMSA experiments

Representative (A) Stains-All- and (B) Coomassie-stained 5% EMSA of TBA or TBA-NNp/DDp in the absence (−) and presence (+) of thrombin (Thr); 130 pmol of each aptamer was incubated with 130, 260, or 65 pmol of the protein, thus obtaining final 1:1, 1:2, or 1:0.5 aptamer-protein molar ratios, respectively. Gels were run, under native conditions, at constant 100 V for 55 min at r.t. in TAE 1X buffer. Lane 1: TBA, lane 2: TBA-thrombin 1:1 complex, lane 3: TBA-thrombin 1:2 complex, lane 4: TBA-thrombin 1:0.5 complex, lane 5: TBA-NNp/DDp, lane 6: TBA-NNp/DDp-thrombin 1:1 complex, lane 7: TBA-NNp/DDp-thrombin 1:2 complex, lane 8: TBA-NNp/DDp-thrombin 1:0.5 complex, lane 9: thrombin.

between the appendages and the protein chain (Figures S15B and S15C). The slightly higher solvent content of the γ form with respect to the β and δ ones can be reasonably justified by the fact that, in this particular case, the ternary complexes are held together in infinite rows by the highly directional stacking interactions between the end-to-end NDI/DAN/NDI/DAN sequence belonging to the aptamer bound to the exosites I and II, respectively (Figure S17). In this rather long stacking sequence, in order to preserve the alternation of NDI and DAN moieties, one of the two intermediate DAN residues is alternatively bulged out and disordered, highlighting the stability of this particular construct. Altogether, the solid-state results strongly suggest that the NDI and DAN end groups favor the binding at exosite II with respect to the parent TBA, in turn leaving essentially unaltered the binding mode at exosite I.

Less definite indications can be obtained from the studies in solution, where the specific properties of the solvent play an important role. Both spectroscopic and calorimetric studies suggested that the compact structure of TBA-NNp/DDp also survives in solution and thermally unfolds according to a one-step mechanism. The specific properties of the terminal moieties affect the determination of the binding stoichiometry of TBA-NNp/DDp to thrombin in solution. In particular, though the isothermal titration calorimetry (ITC) studies performed on the TBA-thrombin system gave a clear-cut indication of the formation of a 1:1 complex, a similar approach with the here investigated TBA analogue provided only a vague indication of the stoichiometry of the complex formed in solution with thrombin (data not shown). However, EMSA analysis revealed a similar behavior for TBA and TBA-NNp/DDp, pointing also for the modified aptamer at the formation of 1:1 protein-aptamer com-

plex. Taken together, these binding data may be interpreted as due to the influence of the end groups that in addition to the more specific interactions, drive toward nonspecific clustering of protein-aptamer molecules, whose contribution depends on the experimental conditions.

The fine-tuning of nucleic-acids hydrophobicity plays a fundamental role in promoting both self-assembly and the formation of complexes with proteins.[53,54] In this context, the detailed structural characterization of the interaction of thrombin with TBA-NNp/DDp has highlighted that the here investigated end-modifications are particularly suitable to modulate the properties of nucleic acids. In particular, their insertion in an oligonucleotide sequence could direct the binding toward the hydrophobic regions of those proteins that still remain difficult targets.

MATERIALS AND METHODS
Materials and sample preparation
The human D-Phe-Pro-Arg-chloromethylketone (PPACK)-inhibited thrombin was purchased from Haematologic Technologies (USA). Unmodified TBA was purchased from biomers.net GmbH (Ulm/Donau, Germany) as HPLC-purified oligomer. Its identity and purity were proved by MALDI-TOF mass spectrometry and HPLC data, as provided by the commercial supplier. TBA-NNp/DDp was synthesized as previously reported.[36] The concentration of the protein and the oligonucleotides was determined by means of UV spectroscopy analysis at 280 nm (at 20°C) and 260 nm (at 90°C), respectively, using molar extinction coefficients calculated from the primary sequences. Prior to each experiment, the aptamer samples were annealed in 10 mM potassium phosphate buffer pH 7.4 and 100 mM KCl by heating to 90°C for 5 min, then slowly cooling down in 50–60 min, and storing at 20°C overnight.

Acrylamide/bis-acrylamide (19:1) 40% solution and glycerol were purchased from VWR. Stains-All, ammonium persulfate (APS), and tetramethylethylenediamine (TEMED) were purchased from Sigma-Aldrich (Merck Life Science S.r.l., Milan, Italy).

Crystallization

The complex between thrombin and TBA-NNp/DDp in 25 mM potassium phosphate buffer pH 7.4 and 100 mM KCl was obtained following a standard protocol.[9] Briefly, a 2-fold molar excess of the aptamer was deposited onto a frozen sample of thrombin and the system was left at 4°C overnight. Finally, the solution was extensively washed and concentrated to about 9 mg mL^{-1} using a 10-kDa-cutoff Centricon mini-concentrator (Vivaspin 500; Sartorius, Goettingen, Germany) and a refrigerated centrifuge (Z216MK; Hermle Labortechnik, Wehingen, Germany).

The initial screening and the optimization of crystallization experiments were performed by the hanging drop vapor diffusion method mixing 0.5 μL complex solution with 0.5 μL reservoir solution at 20°C and reproducing the conditions reported in the literature for the crystallization of other thrombin-aptamer complexes.[9,10,13,14,18,31,37,41–44,55] Crystals suitable for X-ray diffraction data collection grew in four different conditions (Table 1 and Figure S1).

Data collection, structure determination, refinement, and structural analysis

Diffraction data were collected at the XRD2 beamline of Elettra Sincrotrone Trieste (Italy) using λ = 1.0000 Å. Datasets were processed using autoPROC software.[56–59] The phase problem was solved by molecular replacement using Phaser MR[60] from the CCP4 package[58] and the coordinates of the native protein (PDB code: 1PPB),[61] as a search model. Refinement and manual model building were carried out using REFMAC5[58,62] and Coot[63] programs, respectively. Detailed statistics on data collection and refinement are reported in Table S1. Structures were validated using the PDB validation server (https://validate-rcsb-1.wwpdb.org/) and Coot routines.[63] The coordinates of the structures were deposited in the Protein Data Bank (PDB codes: 7ZKL, 7ZKM, 7ZKN, and 7ZKO).

Thrombin-TBA-NNp/DDp interface areas and interactions were examined using the PISA program[64] available online (https://www.ebi.ac.uk/pdbe/pisa/). Molecular graphics figures were generated with PyMOL (DeLano Scientific, Palo Alto, CA, USA).

CD spectroscopy

Circular dichroism (CD) measurements were carried out using a Jasco J-1500 CD spectrometer equipped with a Peltier-type temperature control. Thermal unfolding of a 40 μM aptamer sample was monitored in a 0.1 cm path length cell by following CD changes at 295 nm in the 20–95°C range at the heating rate of 1°C min^{-1}. The melting temperature value was evaluated through analysis of the first derivative of the melting profile.

UV-Vis spectroscopy

UV-Vis experiments were recorded on a Jasco V-770 spectrophotometer equipped with a Peltier thermostatic cell holder, by using a 1 cm path-length cell. The aptamer concentrations were in the range 4.2 to 12 μM. The thermal denaturation curves were obtained by following the UV-Vis signal at 410 nm in the 20–95°C range, at a heating rate of 1.0°C min^{-1}. The melting temperature was determined through analysis of the first derivative of the melting profile.

Differential scanning calorimetry

DSC measurements were performed on a nano-DSC (TA Instruments, USA) equipped with twin capillary cells of a 0.3 mL sensitive volume. A 170 μM TBA-NNp/DDp sample was heated from 5 to 95°C at the scan rate of 1.0°C min^{-1}. The reversibility of the unfolding process was checked by running at least two successive heating and cooling scans at a scanning rate of 1°C min^{-1}. The excess molar heat capacity function was obtained upon subtraction of the baseline, which is assumed to be given by the linear temperature dependence of the native-state heat capacity.[65] A buffer versus buffer scan was subtracted from the sample scan. The melting temperature was determined as the temperature corresponding to the maximum of the thermogram. The unfolding enthalpy, ΔH°, was obtained by direct integration of DSC peak, while the entropy change was obtained by integrating the curve C_p/T versus T (where C_p is the molar heat capacity and T is the temperature in Kelvin).

Electrophoretic mobility shift assay

EMSAs were performed according to reported procedures,[66,67] with minor modifications. In detail, in parallel experiments, 130 pmol of TBA or TBA-NNp/DDp (both previously annealed in 10 mM potassium phosphate buffer pH 7.4 and 100 mM KCl) were mixed with 130, 260, or 65 pmol of thrombin so to have 1:1, 1:2, or 1:0.5 aptamer-protein molar ratio. After incubation for 2 h at 4°C, all the samples were supplemented with glycerol (to a final concentration of 5%) immediately before their loading on the gel and then analyzed by electrophoresis on 5% polyacrylamide gels using TAE (Tris Acetate EDTA) 1X, pH 9.4, as running buffer. Gels were run under native conditions, at constant 100 V and room temperature (r.t.) for 55 min, then stained with Stains-All overnight according to the manufacturer's instructions and finally visualized with a UV transilluminator (BioRad ChemiDoc XRS, Milan, Italy). After DNA staining, the gels were washed in water and stained again with Colloidal Coomassie G-250 to visualize the bands of the free and aptamer-bound protein. Each experiment was performed in triplicate. The intensity of the DNA bands on the gel was then calculated by using the FiJi software and normalized with respect to the free, untreated aptamer. Percentages of the oligonucleotide bands are reported as mean values ±SD for multiple determinations. The statistical significance of replicates was analyzed using Student's t test with *p < 0.1, **p < 0.01, or ***p < 0.001 compared with untreated oligonucleotides.

DATA AVAILABILITY

Atomic coordinates and structure factors for thrombin-TBA-NNp/DDp complex in crystal forms α, β, γ, and δ have been deposited with the Protein Data Bank under accession numbers 7ZKL, 7ZKM, 7ZKN, and 7ZKO, respectively.

SUPPLEMENTAL INFORMATION

Supplemental information can be found online at https://doi.org/10.1016/j.omtn.2022.11.007.

ACKNOWLEDGMENTS

AUTHOR CONTRIBUTIONS

Conceptualization, F.S. and D.M.; validation, F.S., D.M., and P.D.V.; formal analysis, R.T. and C.R.; investigation, R.T., C.R., and K.P.C.; resources, F.S., D.M., P.D.V., M.S., and F.M.; data curation, R.T. and C.R.; writing—original draft, R.T. and F.S.; writing—review and editing, all authors; visualization, R.T. and C.R.; supervision, F.S.; project administration, F.S. and D.M.; funding acquisition, F.S. and D.M. All authors have read and agreed to the published version of the manuscript.

DECLARATION OF INTERESTS

The authors declare no competing interests.

REFERENCES

1. Santosh, B., and Yadava, P.K. (2014). Nucleic acid aptamers: research tools in disease diagnostics and therapeutics. BioMed Res. Int. 2014, 540451.

2. Kotkowiak, W., and Pasternak, A. (2021). Beyond G-quadruplexes—the effect of junction with additional structural motifs on aptamers properties. Int. J. Mol. Sci. 22, 9948.

3. Troisi, R., and Sica, F. (2022). Aptamers: functional-structural studies and biomedical applications. Int. J. Mol. Sci. 23, 4796.

4. Kumar Kulabhusan, P., Hussain, B., and Yüce, M. (2020). Current perspectives on aptamers as diagnostic tools and therapeutic agents. Pharmaceutics 12, 646.

5. Basu, D., Chakraborty, S., Pal, R., Sharma, T.K., and Sarkar, S. (2021). Identification and engineering of aptamers for theranostic application in human health and disorders. Int. J. Mol. Sci. 22, 9661.

6. Hasegawa, H., Savory, N., Abe, K., and Ikebukuro, K. (2016). Methods for improving aptamer binding affinity. Molecules 21, 421.

7. Troisi, R., Balasco, N., Autiero, I., Vitagliano, L., and Sica, F. (2021). Exosite binding in thrombin: a global structural/dynamic overview of complexes with aptamers and other ligands. Int. J. Mol. Sci. 22, 10803.

8. Liu, M., Zaman, K., and Fortenberry, Y.M. (2021). Overview of the therapeutic potential of aptamers targeting coagulation factors. Int. J. Mol. Sci. 22, 3897.

9. Russo Krauss, I., Merlino, A., Randazzo, A., Novellino, E., Mazzarella, L., and Sica, F. (2012). High-resolution structures of two complexes between thrombin and thrombin-binding aptamer shed light on the role of cations in the aptamer inhibitory activity. Nucleic Acids Res. 40, 8119–8128.

10. Troisi, R., Napolitano, V., Spiridonova, V., Russo Krauss, I., and Sica, F. (2018). Several structural motifs cooperate in determining the highly effective anti-thrombin activity of NU172 aptamer. Nucleic Acids Res. 46, 12177–12185.

11. Tasset, D.M., Kubik, M.F., and Steiner, W. (1997). Oligonucleotide inhibitors of human thrombin that bind distinct epitopes. J. Mol. Biol. 272, 688–698.

12. White, R., Rusconi, C., Scardino, E., Wolberg, A., Lawson, J., Hoffman, M., and Sullenger, B. (2001). Generation of species cross-reactive aptamers using "toggle" SELEX. Mol. Ther. 4, 567–573.

13. Long, S.B., Long, M.B., White, R.R., and Sullenger, B.A. (2008). Crystal structure of an RNA aptamer bound to thrombin. RNA 14, 2504–2512.

14. Russo Krauss, I., Pica, A., Merlino, A., Mazzarella, L., and Sica, F. (2013). Duplex-quadruplex motifs in a peculiar structural organization cooperatively contribute to thrombin binding of a DNA aptamer. Acta Crystallogr. D Biol. Crystallogr. 69, 2403–2411.

15. Müller, J., Freitag, D., Mayer, G., and Pötzsch, B. (2008). Anticoagulant characteristics of HD1-22, a bivalent aptamer that specifically inhibits thrombin and prothrombinase. J. Thromb. Haemost. 6, 2105–2112.

16. Feng, X., Yu, C., Feng, F., Lu, P., Chai, Y., Li, Q., et al. (2019). Direct measurement of through-bond effects in molecular multivalent interactions. Chem. Eur. J. 25, 2978–2982.

17. Troisi, R., Balasco, N., Vitagliano, L., and Sica, F. (2021). Molecular dynamics simulations of human α-thrombin in different structural contexts: evidence for an aptamer-guided cooperation between the two exosites. J. Biomol. Struct. Dyn. 39, 2199–2209.

18. Troisi, R., Balasco, N., Santamaria, A., Vitagliano, L., and Sica, F. (2021). Structural and functional analysis of the simultaneous binding of two duplex/quadruplex aptamers to human α-thrombin. Int. J. Biol. Macromol. 181, 858–867.

19. Haßel, S.K., and Mayer, G. (2019). Aptamers as therapeutic agents: has the initial euphoria subsided? Mol. Diagn. Ther. 23, 301–309.

20. Peng, C.G., and Damha, M.J. (2007). G-quadruplex induced stabilization by 2'-deoxy-2'-fluoro-D-arabinonucleic acids (2'F-ANA). Nucleic Acids Res. 35, 4977–4988.

21. Borbone, N., Bucci, M., Oliviero, G., Morelli, E., Amato, J., D'Atri, V., D'Errico, S., Vellecco, V., Cirino, G., Piccialli, G., et al. (2012). Investigating the role of T7 and T12 residues on the biological properties of thrombin-binding aptamer: enhancement of anticoagulant activity by a single nucleobase modification. J. Med. Chem. 55, 10716–10728.

22. Virgilio, A., Petraccone, L., Scuotto, M., Vellecco, V., Bucci, M., Mayol, L., Varra, M., Esposito, V., and Galeone, A. (2014). 5-Hydroxymethyl-2'-deoxyuridine residues in the thrombin binding aptamer: investigating anticoagulant activity by making a tiny chemical modification. Chembiochem 15, 2427–2434.

23. Kotkowiak, W., Lisowiec-Wachnicka, J., Grynda, J., Kierzek, R., Wengel, J., and Pasternak, A. (2018). Thermodynamic, anticoagulant, and antiproliferative properties of thrombin binding aptamer containing novel UNA derivative. Mol. Ther. Nucleic Acids 10, 304–316.

24. Ying, G., Lu, X., Mei, J., Zhang, Y., Chen, J., Wang, X., Ou, Z., and Yi, Y. (2019). A structure-activity relationship of a thrombin-binding aptamer containing LNA in novel sites. Bioorg. Med. Chem. 27, 3201–3207.

25. Aviñó, A., Jorge, A.F., Huertas, C.S., Cova, T.F.G.G., Pais, A., Lechuga, L.M., Eritja, R., and Fabrega, C. (2019). Aptamer-peptide conjugates as a new strategy to modulate human α-thrombin binding affinity. Biochim. Biophys. Acta Gen. Subj. 1863, 1619–1630.

26. De Fenza, M., Eremeeva, E., Troisi, R., Yang, H., Esposito, A., Sica, F., et al. (2020). Structure-activity relationship study of a potent α-thrombin binding aptamer incorporating hexitol nucleotides. Chem. Eur. J. 26, 9589–9597.

27. Kovačič, M., Podbevšek, P., Tateishi-Karimata, H., Takahashi, S., Sugimoto, N., and Plavec, J. (2020). Thrombin binding aptamer G-quadruplex stabilized by pyrene-modified nucleotides. Nucleic Acids Res. 48, 3975–3986.

28. Varada, M., Aher, M., Erande, N., Kumar, V.A., and Fernandes, M. (2020). Methoxymethyl threofuranosyl thymidine (4'-MOM-TNA-T) at the T7 position of the thrombin-binding aptamer boosts anticoagulation activity, thermal stability, and nuclease resistance. ACS Omega 5, 498–506.

29. Riccardi, C., Napolitano, E., Platella, C., Musumeci, D., and Montesarchio, D. (2021). G-quadruplex-based aptamers targeting human thrombin: discovery, chemical modifications and antithrombotic effects. Pharmacol. Ther. 217, 107649.

30. Kotkowiak, W., Jahnz-Wechmann, Z., and Pasternak, A. (2021). A comprehensive analysis of the thrombin binding aptamer containing functionalized pyrrolo-2'-deoxycytidines. Pharmaceuticals 14, 1326.

31. Smirnov, I., Kolganova, N., Troisi, R., Sica, F., and Timofeev, E. (2021). Expanding the recognition interface of the thrombin-binding aptamer HD1 through modification of residues T3 and T12. Mol. Ther. Nucleic Acids 23, 863–871.

32. Bao, H.-L., Ishizuka, T., Yamashita, A., Furukoji, E., Asada, Y., and Xu, Y. (2021). Improving thermodynamic stability and anticoagulant activity of a thrombin binding aptamer by incorporation of 8-trifluoromethyl-2'-deoxyguanosine. J. Med. Chem. 64, 711–718.

33. Riccardi, C., Meyer, A., Vasseur, J.-J., Russo Krauss, I., Paduano, L., Oliva, R., Petraccone, L., Morvan, F., and Montesarchio, D. (2019). Stability is not everything: the case of the cyclisation of a thrombin-binding aptamer. Chembiochem 20, 1789–1794.

34. Riccardi, C., Meyer, A., Vasseur, J.-J., Russo Krauss, I., Paduano, L., Morvan, F., and Montesarchio, D. (2020). Fine-tuning the properties of the thrombin binding aptamer through cyclization: effect of the 5'-3' connecting linker on the aptamer stability and anticoagulant activity. Bioorg. Chem. 94, 103379.

35. Riccardi, C., Meyer, A., Vasseur, J.-J., Cavasso, D., Russo Krauss, I., Paduano, L., Morvan, F., and Montesarchio, D. (2020). Design, synthesis and characterization of cyclic NU172 analogues: a biophysical and biological insight. Int. J. Mol. Sci. 21, E3860.

36. Pérez de Carvasal, K., Riccardi, C., Russo Krauss, I., Cavasso, D., Vasseur, J.-J., Smietana, M., Morvan, F., and Montesarchio, D. (2021). Charge-transfer interactions stabilize G-quadruplex-forming thrombin binding aptamers and can improve their anticoagulant activity. Int. J. Mol. Sci. 22, 9510.

37. Russo Krauss, I., Spiridonova, V., Pica, A., Napolitano, V., and Sica, F. (2016). Different duplex/quadruplex junctions determine the properties of anti-thrombin aptamers with mixed folding. Nucleic Acids Res. 44, 983–991.

38. Padmanabhan, K., and Tulinsky, A. (1996). An ambiguous structure of a DNA 15-mer thrombin complex. Acta Crystallogr. D Biol. Crystallogr. 52, 272–282.

39. Russo Krauss, I., Napolitano, V., Petraccone, L., Troisi, R., Spiridonova, V., Mattia, C.A., and Sica, F. (2018). Duplex/quadruplex oligonucleotides: role of the duplex domain in the stabilization of a new generation of highly effective anti-thrombin aptamers. Int. J. Biol. Macromol. 107, 1697–1705.

40. Hellman, L.M., and Fried, M.G. (2007). Electrophoretic mobility shift assay (EMSA) for detecting protein-nucleic acid interactions. Nat. Protoc. 2, 1849–1861.

41. Russo Krauss, I., Merlino, A., Giancola, C., Randazzo, A., Mazzarella, L., and Sica, F. (2011). Thrombin-aptamer recognition: a revealed ambiguity. Nucleic Acids Res. 39, 7858–7867.

42. Pica, A., Russo Krauss, I., Merlino, A., Nagatoishi, S., Sugimoto, N., and Sica, F. (2013). Dissecting the contribution of thrombin exosite I in the recognition of thrombin binding aptamer. FEBS J. 280, 6581–6588.

43. Pica, A., Russo Krauss, I., Parente, V., Tateishi-Karimata, H., Nagatoishi, S., Tsumoto, K., Sugimoto, N., and Sica, F. (2017). Through-bond effects in the ternary complexes of thrombin sandwiched by two DNA aptamers. Nucleic Acids Res. 45, 461–469.

44. Dolot, R., Lam, C.H., Sierant, M., Zhao, Q., Liu, F.-W., Nawrot, B., Egli, M., and Yang, X. (2018). Crystal structures of thrombin in complex with chemically modified thrombin DNA aptamers reveal the origins of enhanced affinity. Nucleic Acids Res. 46, 4819–4830.

45. Trapaidze, A., Bancaud, A., and Brut, M. (2015). Binding modes of thrombin binding aptamers investigated by simulations and experiments. Appl. Phys. Lett. 106, 043702.

46. Trapaidze, A., Hérault, J.-P., Herbert, J.-M., Bancaud, A., and Gué, A.-M. (2016). Investigation of the selectivity of thrombin-binding aptamers for thrombin titration in murine plasma. Biosens. Bioelectron. 78, 58–66.

47. Gabriel, G.J., and Iverson, B.L. (2002). Aromatic oligomers that form hetero duplexes in aqueous solution. J. Am. Chem. Soc. 124, 15174–15175.

48. Ikkanda, B.A., Samuel, S.A., and Iverson, B.L. (2014). NDI and DAN DNA: nucleic acid-directed assembly of NDI and DAN. J. Org. Chem. 79, 2029–2037.

49. Prentice, G.M., Pascu, S.I., Filip, S.V., West, K.R., and Pantoş, G.D. (2015). Aromatic donor–acceptor interactions in non-polar environments. Chem. Commun. 51, 8265–8268.

50. Ikkanda, B.A., and Iverson, B.L. (2016). Exploiting the interactions of aromatic units for folding and assembly in aqueous environments. Chem. Commun. 52, 7752–7759.

51. Pérez de Carvasal, K., Aissaoui, N., Vergoten, G., Bellot, G., Vasseur, J.-J., Smietana, M., and Morvan, F. (2021). Folding of phosphodiester-linked donor-acceptor oligomers into supramolecular nanotubes in water. Chem. Commun. 57, 4130–4133.

52. Takada, T., Otsuka, Y., Nakamura, M., and Yamana, K. (2014). Formation of a charge transfer complex within a hydrophobic cavity in DNA. RSC Adv. 4, 59440–59443.

53. Davies, D.R., Gelinas, A.D., Zhang, C., Rohloff, J.C., Carter, J.D., O'Connell, D., Waugh, S.M., Wolk, S.K., Mayfield, W.S., Burgin, A.B., et al. (2012). Unique motifs and hydrophobic interactions shape the binding of modified DNA ligands to protein targets. Proc. Natl. Acad. Sci. USA 109, 19971–19976.

54. Xiao, F., Chen, Z., Wei, Z., and Tian, L. (2020). Hydrophobic interaction: a promising driving force for the biomedical applications of nucleic acids. Adv. Sci. 7, 2001048.

55. Abeydeera, N.D., Egli, M., Cox, N., Mercier, K., Conde, J.N., Pallan, P.S., Mizurini, D.M., Sierant, M., Hibti, F.-E., Hassell, T., et al. (2016). Evoking picomolar binding in RNA by a single phosphorodithioate linkage. Nucleic Acids Res. 44, 8052–8064.

56. Evans, P. (2006). Scaling and assessment of data quality. Acta Crystallogr. D Biol. Crystallogr. 62, 72–82.

57. Kabsch, W. (2010). Xds. Acta Crystallogr. D Biol. Crystallogr. 66, 125–132.

58. Winn, M.D., Ballard, C.C., Cowtan, K.D., Dodson, E.J., Emsley, P., Evans, P.R., et al. (2011). Overview of the CCP4 suite and current developments. Acta Crystallogr. D Biol. Crystallogr. 67, 235–242.

59. Vonrhein, C., Flensburg, C., Keller, P., Sharff, A., Smart, O., Paciorek, W., et al. (2011). Data processing and analysis with the autoPROC toolbox. Acta Crystallogr. D Biol. Crystallogr. 67, 293–302.

60. McCoy, A.J., Grosse-Kunstleve, R.W., Adams, P.D., Winn, M.D., Storoni, L.C., and Read, R.J. (2007). Phaser crystallographic software. J. Appl. Crystallogr. 40, 658–674.

61. Bode, W., Turk, D., and Karshikov, A. (1992). The refined 1.9-A X-ray crystal structure of D-Phe-Pro-Arg chloromethylketone-inhibited human alpha-thrombin: structure analysis, overall structure, electrostatic properties, detailed active-site geometry, and structure-function relationships. Protein Sci. 1, 426–471.

62. Murshudov, G.N., Skubák, P., Lebedev, A.A., Pannu, N.S., Steiner, R.A., Nicholls, R.A., et al. (2011). REFMAC5 for the refinement of macromolecular crystal structures. Acta Crystallogr. D Biol. Crystallogr. 67, 355–367.

63. Emsley, P., Lohkamp, B., Scott, W.G., and Cowtan, K. (2010). Features and development of Coot. Acta Crystallogr. D Biol. Crystallogr. 66, 486–501.

64. Krissinel, E., and Henrick, K. (2007). Inference of macromolecular assemblies from crystalline state. J. Mol. Biol. 372, 774–797.

65. Pagano, B., Randazzo, A., Fotticchia, I., Novellino, E., Petraccone, L., and Giancola, C. (2013). Differential scanning calorimetry to investigate G-quadruplexes structural stability. Methods 64, 43–51.

66. Moccia, F., Riccardi, C., Musumeci, D., Leone, S., Oliva, R., Petraccone, L., and Montesarchio, D. (2019). Insights into the G-rich VEGF-binding aptamer V7t1: when two G-quadruplexes are better than one. Nucleic Acids Res. 47, 8318–8331.

67. Riccardi, C., Musumeci, D., Platella, C., Gaglione, R., Arciello, A., and Montesarchio, D. (2020). Tuning the polymorphism of the anti-VEGF G-rich V7t1 aptamer by covalent dimeric constructs. Int. J. Mol. Sci. 21, 1963.